PAPER • **OPEN ACCESS**

Towards range-guidance in proton therapy to detect organ motion-induced dose degradations

To cite this article: Kia Busch *et al* 2022 *Biomed. Phys. Eng. Express* **8** 025018

Biomedical Physics & Engineering Express

PAPER

Towards range-guidance in proton therapy to detect organ motion-induced dose degradations

Kia Busch[1,2,6], **Andreas G Andersen**[1,2,6], **Jørgen B B Petersen**[1,3], **Stine E Petersen**[1], **Heidi S Rønde**[1], **Lise Bentzen**[2,3], **Sara Pilskog**[4,5], **Peter Skyt**[1], **Ole Nørrevang**[1] **and Ludvig P Muren**[1,2]

[1] Danish Centre for Particle Therapy, Aarhus University Hospital, Aarhus, Denmark
[2] Department of Clinical Medicine, Aarhus University, Aarhus, Denmark
[3] Department of Oncology, Aarhus University Hospital, Aarhus, Denmark
[4] Department of Physics and Technology, University of Bergen, Norway
[5] Department of Oncology and Medical Physics, Haukeland University Hospital, Bergen, Norway
[6] These authors contributed equally

E-mail: ludvmure@rm.dk

Keywords: range-guidance, water equivalent path length, advanced prostate cancer, proton therapy, inter-fractional motion

Supplementary material for this article is available online

OPEN ACCESS

RECEIVED
25 November 2021

REVISED
26 January 2022

ACCEPTED FOR PUBLICATION
2 February 2022

PUBLISHED
18 February 2022

Abstract

Introduction. Internal organ motion and deformations may cause dose degradations in proton therapy (PT) that are challenging to resolve using conventional image-guidance strategies. This study aimed to investigate the potential of *range guidance* using water-equivalent path length (WEPL) calculations to detect dose degradations occurring in PT. *Materials and methods.* Proton ranges were estimated using WEPL calculations. Field-specific isodose surfaces in the planning CT (pCT), from robustly optimised five-field proton plans (opposing lateral and three posterior/posterior oblique beams) for locally advanced prostate cancer patients, were used as starting points. WEPLs to each point on the field-specific isodoses in the pCT were calculated. The corresponding range for each point was found in the repeat CTs (rCTs). The spatial agreement between the resulting surfaces in the rCTs (hereafter referred to as iso-WEPLs) and the isodoses re-calculated in rCTs was evaluated for different dose levels and Hausdorff thresholds (2–5 mm). Finally, the sensitivity and specificity of detecting target dose degradation (V95% $<$ 95%) using spatial agreement measures between the iso-WEPLs and isodoses in the pCT was evaluated. *Results.* The spatial agreement between the iso-WEPLs and isodoses in the rCTs depended on the Hausdorff threshold. The agreement was 65%–88% for a 2 mm threshold, 83%–96% for 3 mm, 90%–99% for 4 mm, and 94%–99% for 5 mm, across all fields and isodose levels. Minor differences were observed between the different isodose levels investigated. Target dose degradations were detected with 82%–100% sensitivity and 75%–80% specificity using a 2 mm Hausdorff threshold for the lateral fields. *Conclusion.* Iso-WEPLs were comparable to isodoses re-calculated in the rCTs. The proposed strategy could detect target dose degradations occurring in the rCTs and could be an alternative to a fully-fledged dose re-calculation to detect anatomical variations severely influencing the proton range.

Introduction

The development of optimal image-guidance strategies in proton therapy (PT) to account for anatomical changes and secure target coverage is challenged by the increased sensitivity of protons to density changes along the beam path, compared to conventional radiotherapy [1, 2]. Conventional image guidance in PT uses kV planar x-ray images or cone-beam CTs (CBCT) to align the patient on bony or soft tissue anatomy. Patient set-up variations, internal organ motion, and density changes along the proton beam paths should be addressed before fraction delivery to secure target coverage and reduce the dose to normal tissues. Various online daily image guidance and plan adaptation strategies have been investigated [3], such as restoring or re-optimising the treatment plan or the use of dose-guided PT, where daily patient positioning is selected

based on the most optimal dose distribution [4–7]. These methods rely on the re-delineation of targets or normal tissues. However, water-equivalent path length (WEPL) calculations could potentially estimate if anatomical variations have influenced the proton range without the need for re-delineations. This method, performed on volumetric images acquired before a treatment fraction, could detect if target dose degradations will occur and indicate the need for plan adaptations.

WEPL calculations have been investigated previously, e.g. to identify robust PT beam orientations for various tumour sites [8–11]. Other studies have exploited the speed and simplicity of WEPL calculations to investigate changes in proton ranges during treatment [12, 13]. Santiago *et al* concluded that fast online analysis of WEPL variations could be combined with image guidance in PT for lung cancer to detect anatomical changes [12]. Kim *et al* investigated the use of WEPL calculations to the distal end of the target for head and neck cancer patients. They showed that dose variations due to anatomical changes and patient set-up could be determined using WEPL to measure range variations [13]. However, this method does not scale well with large volumes. Furthermore, standard WEPL calculations are hard to visualise, and the impact on dose distributions are difficult to estimate. Meanwhile, the alternative of fully-fledged dose re-calculations, even with fast dose calculation engines, requires re-delineation and time-consuming quality assurance.

Therefore, our study aimed to investigate if range/WEPL variations away from the planned isodose distributions, thereby eliminating the need for target re-delineation, can be used to indicate organ motion-induced dose degradations requiring modifications before treatment in PT.

Materials and methods

Water-equivalent path length calculations

Proton ranges were estimated by an in-house developed method for WEPL calculations using isodose structures as the starting point. Initially, dose distributions were calculated using a proton convolution superposition algorithm (Version 13.7.21) from the Eclipse treatment planning system (TPS) (Version 13.7, Varian Medical Systems, Palo Alto, CA, USA). WEPLs were subsequently calculated from each point at the distal surface of the isodose structures in the field direction in the planning CT (pCT) until the edge of the pCT image. They were computed as line integrals through the CT image in the direction of the respective treatment fields. I.e. as a sum of stopping-power values translated from the Hounsfield unit (HU) values applying the look-up table used clinically at the Danish Centre for Particle Therapy (Suppl. Mat. A). Afterwards, the reverse line integrals were calculated into the repeat CTs (rCTs) from the edge of the image until the corresponding WEPL values were reached. This method produces a corresponding isodose-based WEPL contour (hereafter referred to as iso-WEPL) in the rCTs. Only the distal points were considered in the iso-WEPL analysis (Suppl. Mat. B).

The above method was implemented in C^{++} as an integral part of a more extensive open-source application [14, 15]. At each step through the CT images, the values were extracted by linear interpolation, with a step size of 0.1 mm. As the application loaded the images through the Insight Toolkit (ITK) [16], the built-in ITK methods were used for convenience. The implementation was mainly optimised by vectorisation and pre-calculating values before looping to avoid more expensive operations in the inner loops. There is thus still room for optimising the algorithm further, e.g., by parallelisation.

Patient cohort

Eight locally advanced prostate cancer patients originally treated with radiotherapy (RT) at Haukeland University Hospital, Norway, during 2007 were included in this study. The patients were part of a clinical study approved by the relevant ethics committee [17]. Each patient had a pCT and 8–10 rCTs (2–3 mm slice thickness) [18]. Seven patients had bladder contrast in the pCT that was overwritten to the mean HU of the bladder in each patient's first rCT.

Two experienced radiation oncologists contoured the targets and relevant organs at risk (OARs) on pCTs and rCTs using the Eclipse TPS. The lymph node target and bowel contouring are described in Busch *et al* [19]. Additional details are described by Thörnqvist *et al* [18].

Treatment planning

Five-field intensity-modulated proton therapy (IMPT) plans using multi-field worst-case optimisation were created for each patient using the Eclipse TPS. Two lateral opposed fields at 90 and 270 degrees targeted the prostate and seminal vesicles. Additionally, three posterior/posterior-oblique fields at 150, 180 and 210 degrees targeted the lymph nodes [20]. For the robust optimisation, an isocenter shift of 5 mm and a range uncertainty of 3.5% were used on the CTVs. The prescribed dose was 78 Gy (RBE) for the prostate CTV (p-CTV) and 56 Gy (RBE) for the lymph node and seminal vesicle CTV (ln/sv-CTV), delivered in 39 fractions. A relative biological effectiveness of 1.1 was assumed for all doses presented in this paper. When approving the plans, the in-house photon-based clinical protocols were used for the OARs (suppl. Mat. C). Additionally, D95% $\geqslant$ 98% were used for the CTVs and the uncertainty scenarios instead of the PTV constraints. A senior clinical medical physicist approved all plans. The plans were re-calculated on the rCTs after a bony-anatomy based rigid registration. Changes in bony-anatomy have previously been identified as a significant cause of dose deterioration [6, 10].

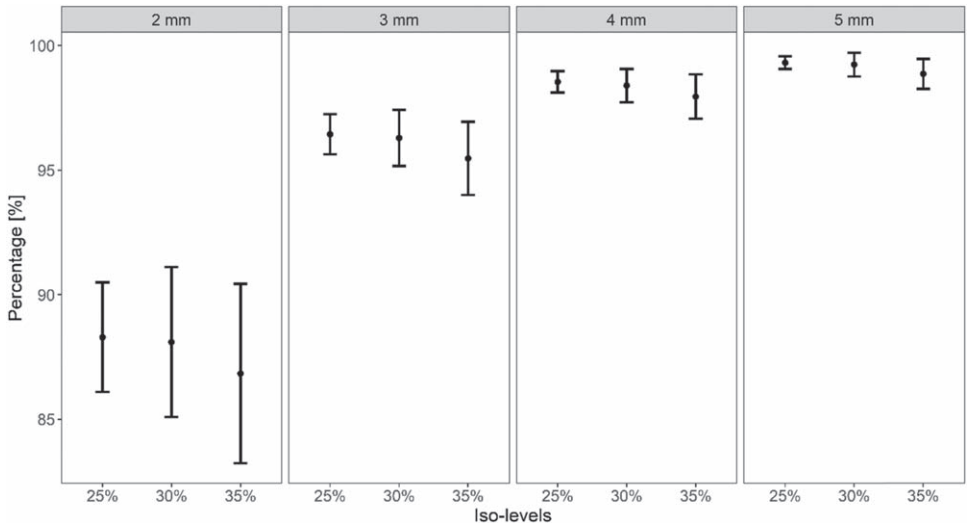

Figure 1. Estimated mean spatial agreement and 95% confidence interval between the iso-WEPLs and isodoses in the rCTs for a Hausdorff threshold of 2, 3, 4 and 5 mm and three iso-levels for the fields at 90 degrees across all patients and rCTs.

Analysis of water-equivalent path length and dose changes

Iso-WEPLs were calculated for each field using dose levels that corresponded roughly to the contribution from each field to the total dose. For the posterior/posterior-oblique fields, iso-WEPLs were calculated using 15%, 20% and 25% of the 78 Gy prescription dose level for the primary target, along with 25%, 30% and 35% for each of the laterally opposed beams. These levels were chosen by examining the individual fields to find the approximate relative contributions. The original isodoses in the pCT and rCTs were calculated for each field using the CERR platform in MATLAB (The MathWorks Inc., Natick, MA, USA) based on a dose distribution from Eclipse TPS.

The iso-WEPLs were initially compared to the isodose surfaces from a fully-fledged dose re-calculation in the rCTs. The spatial agreement was evaluated as the percentage of points below certain Hausdorff distances, 2, 3, 4 and 5 mm. The distances were calculated between the iso-WEPLs and the isodoses. A linear mixed-effect model was used to estimate the mean spatial agreement and 95% confidence interval (95%CI) of the percentage of points below a certain Hausdorff threshold across patients and rCTs. Normality was assessed from a quantile-quantile plot of the residuals.

The relation between target dose degradation and the difference between the iso-WEPLs in the rCTs and the isodoses in the pCT were investigated to explore the use of range variations as an indicator for target dose degradations caused by inter-fractional organ motion. Target dose degradations were defined as cases where the target volume received less than 95% of the prescribed dose (V95%) for the p-CTV and ln/sv-CTV. Iso-WEPL classification potential was evaluated and assessed by calculating the sensitivity (true positive rate), specificity (true negative rate), positive predictive values (PPV) as well as negative predictive values (NPV) with a threshold of 95% for V95% and an investigation based threshold of 90% for the spatial agreement between the iso-WEPL and isodoses in the pCTs.

Results

The spatial agreement between the iso-WEPLs and the isodoses from the calculated dose distributions in the rCTs mainly correlated with the Hausdorff threshold explored. In contrast, the different iso-levels had a minor impact (within 1%) (figures 1 and 2). For a Hausdorff threshold of 2 mm, the highest estimated mean spatial agreement was 88% (95%CI: 86%–91%), i.e., on average, 88% of the points in the iso-WEPLs were less than 2 mm away from a point in the distal surface of the rCT isodose, across all patients and rCTs; this was for a 25% iso-level and the field at 90 degrees (figure 1). For this iso-level and field direction, the mean spatial agreement measure increased to 96% (95%CI: 96%–97%) for a 3 mm threshold and 99% for both 4 mm and 5 mm thresholds (95%CIs were 98%–99% and 99%–100% respectively). Similar results were seen for the field at 270 degrees (Suppl. Mat. D).

The lowest estimated mean spatial agreement of 65% (95%CI: 58%–72%) occurred for a threshold of 2 mm and a 25% iso-level for the left posterior oblique field at 150 degrees (figure 2). For this iso-level and field direction, the estimated mean spatial agreement was 83% (95%CI: 79%–87%) for a 3 mm threshold, 90% (95%CI: 87%–93%) for a 4 mm threshold and 94% (95%CI: 91%–97%) for a 5 mm threshold. These lower median values were caused mainly by small displacements of the pCT and rCT isodoses (Suppl. Mat. E). Comparatively, the lateral field results were affected less due to the direction of the displacement. The same trend was observed for the fields at 180 and 210 degrees (Suppl. Mat. D).

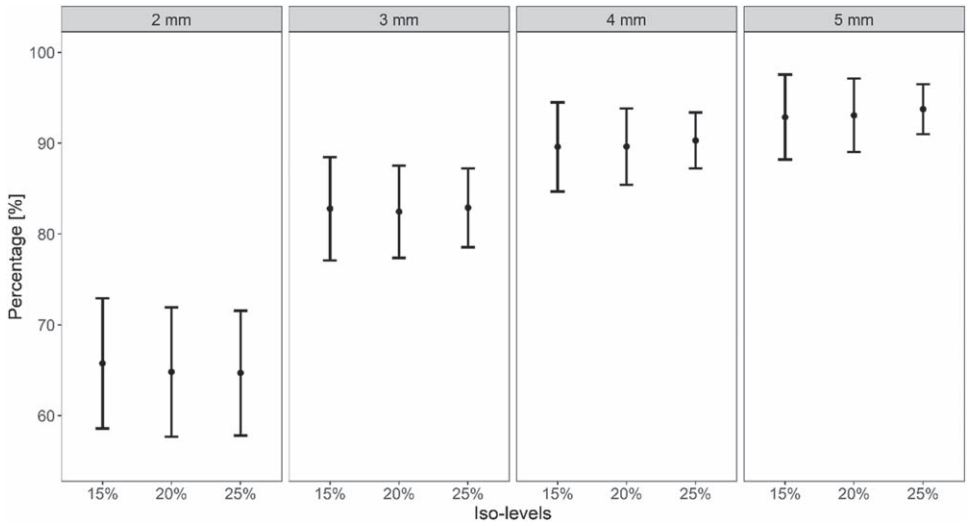

Figure 2. Estimated mean spatial agreement and 95% confidence interval between the iso-WEPLs and isodoses in the rCTs for a Hausdorff threshold of 2, 3, 4 and 5 mm and three iso-levels for the fields at 150 degrees across all patients and rCTs.

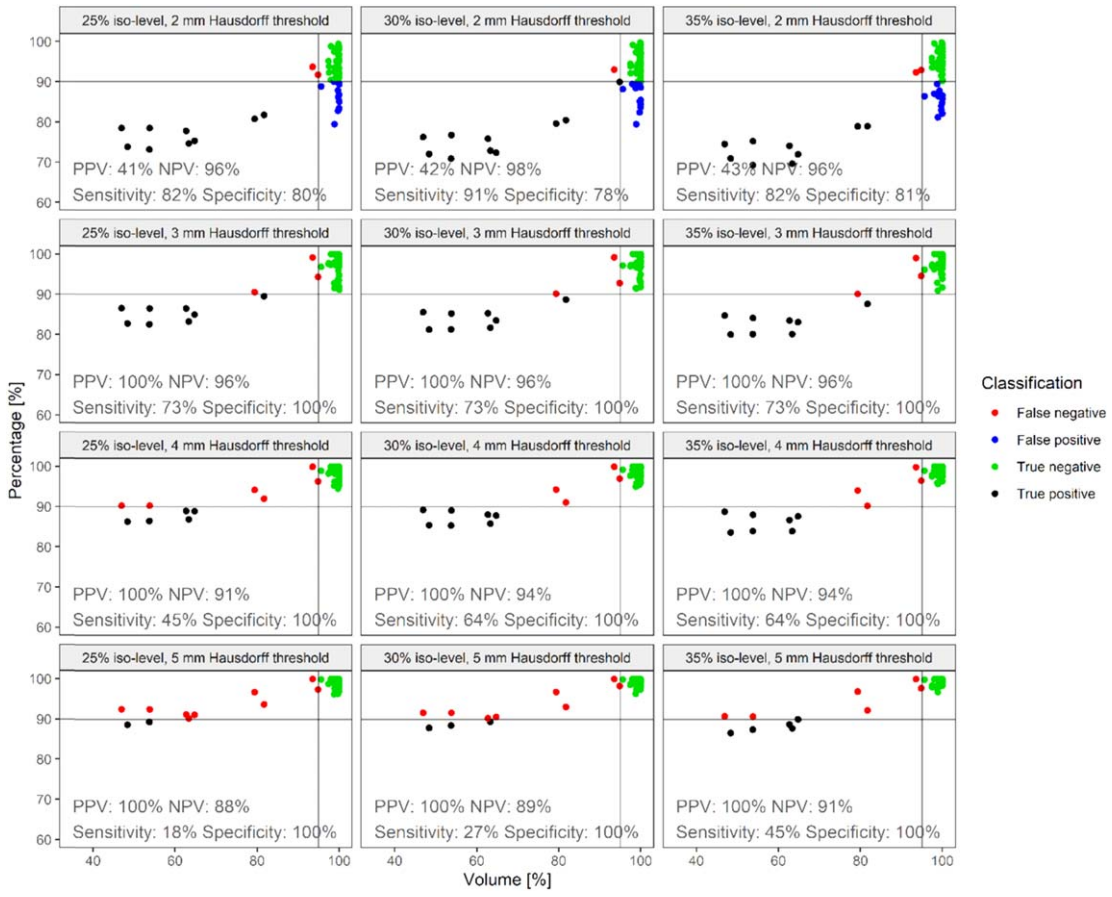

Figure 3. V95% for the p-CTV in the rCTs against the spatial agreement with Hausdorff thresholds of 2, 3, 4 and 5 mm for the field at 270 degrees. The spatial agreement is calculated between the iso-WEPLs and the isodoses in the pCT at three iso-levels.

Range variations as an indicator for dose deterioration

We were able to detect dose degradation in the p-CTV through range variations between the iso-WEPLs and the isodoses in the pCT, particularly when using a 2–3 mm Hausdorff threshold (figure 3). E.g. for the field at 270 degrees, using a 2 mm Hausdorff threshold and a 25% iso-level resulted in 82% sensitivity, 80% specificity, and 96% NPV, yet a PPV of only 41%. For a 5 mm Hausdorff threshold, the sensitivity was 18%. However, the specificity was 100%, PPV was 100%, and the NPV was 88%. As for comparing the iso-WEPLs and isodoses in the pCTs, the differences between the iso-levels were minor, resulting in similar values for the sensitivity, specificity,

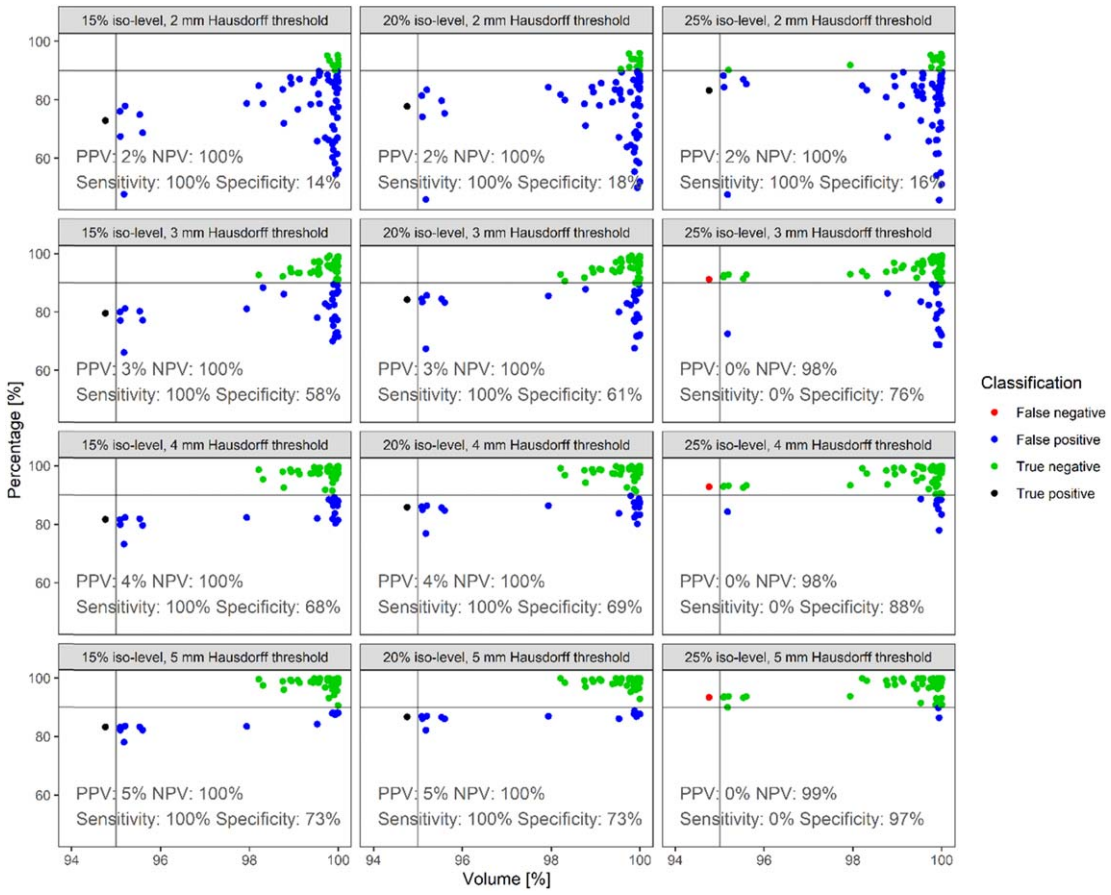

Figure 4. V95% for the ln/sv-CTV in the rCTs against the spatial agreement with Hausdorff thresholds of 2, 3, 4 and 5 mm for the field at 150 degrees. The spatial agreement is calculated between the iso-WEPLs and the isodoses in the pCT at three iso-levels.

PPV and NPV. True positives were also captured using a 2 mm Hausdorff threshold for the field at 90 degrees, resulting in 100% sensitivity, 75% specificity, 41% PPV and 100% NPV for a 25% iso-level. However, the sensitivity decreased to 0%–18% when the Hausdorff threshold increased. For a 25% iso-level using a 5 mm threshold, the specificity was 100%, and the NPV was 85%. Here, it was not possible to calculate the PPV because no true or false positives were detected. Similar to the field at 270 degrees, minor variations were observed between iso-levels (Suppl. Mat. F). The most considerable dose degradation for the p-CTV was observed in one patient with air present in the rectum in the pCT, which was not present in the rCTs (figure 5).

The ln/sv-CTV showed good target coverage in most rCTs, resulting in a low number of true positives and false negatives (figure 4). Across all Hausdorff thresholds and iso-levels, the PPV was 0%–5%, but the NPV was 98%–100% for the field at 150 degrees. The sensitivity was 100%, except for at the 25% iso-level using a 3–5 mm Hausdorff threshold where the sensitivity was 0% because of no true positives. The specificity varied between Hausdorff thresholds and iso-levels with a range of 14%–97%, as the number of false positives varied. The same trend was observed for the other posterior/posterior-oblique fields (Suppl. Mat. F).

Discussion

This study investigated if range variations based on WEPL calculations can detect organ motion-induced dose degradation. The WEPL-based isodoses agreed well spatially with the isodoses in the rCTs. This agreement indicates that WEPL calculations can be an alternative to a fully-fledged dose re-calculation. Dose degradations were identified by comparing the WEPL-based isodoses with the isodoses in the pCTs.

When comparing iso-WEPLs with isodoses in the rCTs, the spatial agreement increased as expected with the Hausdorff threshold, reaching almost 100% for a 5 mm threshold. At the same time, the iso-levels were found to have a more negligible impact on the spatial agreement. However, target dose deterioration was detected for Hausdorff thresholds of 2–3 mm.

The optimal Hausdorff threshold depended on both the gantry angles and target dose constraints selected, influencing the sensitivity, specificity, PPV and NPV results. It will therefore be necessary to investigate various Hausdorff thresholds for different tumour sites properly. Finding the optimal Hausdorff threshold is a balance between capturing all cases where dose deterioration occurs (high sensitivity) and having a high specificity method. A high sensitivity target will most likely result in a higher number of false

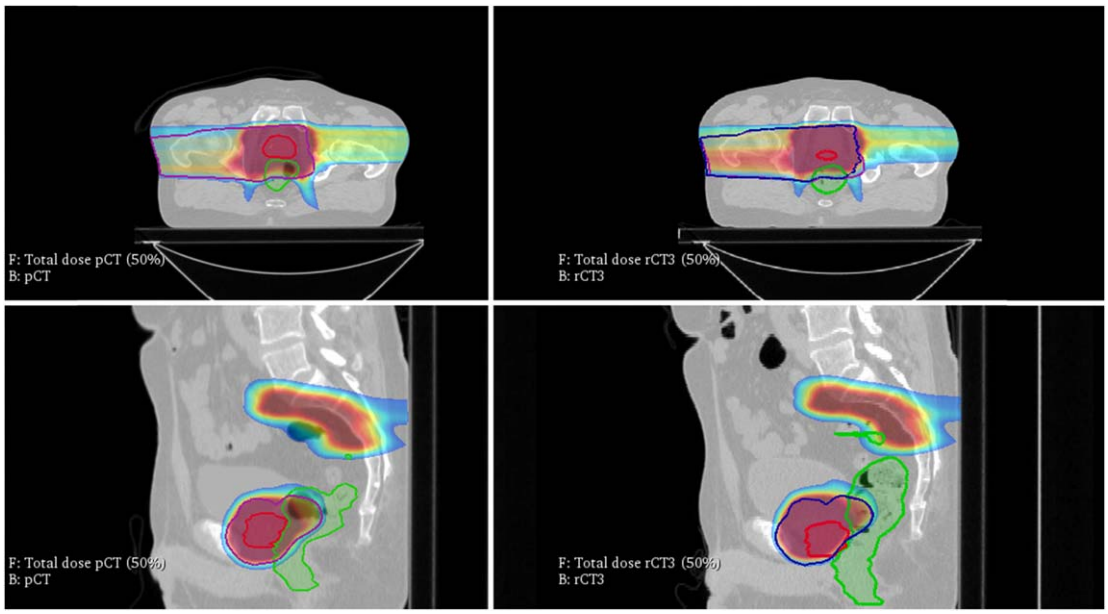

Figure 5. Comparison of pCT (left) and rCT (right) doses and iso-contours. The total dose is shown as a colour wash overlaid with the prostate (red) and rectum (green) structures as well as the pCT isodose (purple) and the iso-WEPL (blue). The top and bottom row is the axial and sagittal views, respectively. Patient 3 is shown with the third rCT; iso-contours are for a field of 270-degree gantry angle at 25% of the prescription dose.

positives. In contrast, a high specificity target may result in a higher number of false negatives. In addition, the plan optimisation method may also influence the results. It should be pointed out that the plans in this study were made to be as close to clinical practice as possible, focusing on plan robustness. The multi-field optimisation used in this study makes it difficult to select iso-levels to explore since the field-specific dose distributions are inhomogeneous. Although, when combined, they cover the target [21].

Overall a lower agreement was observed for the iso-contours with a large surface (the oblique fields), which may cause the WEPL approximation to become more inaccurate. Minor displacements between the pCT and rCT isodoses also caused the iso-WEPLs to differ from those in the rCTs (See Suppl. Mat. E). This displacement was possibly caused by forced dose matrix or isodose alignment with the CT grid in either Eclipse, CERR or both. With a slice-thickness of 3 mm, this can add up to a significant error for large structures. In addition, WEPL calculations do not account for any scatter or lateral spread of the beam. WEPL is a directional measure calculating the range along a specific line.

Furthermore, range guidance based on WEPL calculations handles each field individually, not accounting for inhomogeneous field-specific dose distributions. The individual fields have a different spot weight distribution and a different contribution to the total dose, which is not accounted for in our method. This difference is also why the results between range and dose degradation varied between the fields. This study used the distal surface of isodoses of different levels as the starting points for the WEPL calculations as a simplified approach. However, to account for inhomogeneous field doses, a cost function could be implemented that weighs the importance of range variations for different positions for each field-specific dose distribution based on the contribution to the total dose.

Previous studies using range calculations to study the effect of anatomical variations have calculated WEPL differences for fixed points and then analysed, e.g. the average or root-mean-square deviation across the points [9, 11–13]. We found that such a method would not capture the differences in range with sufficient sensitivity when scaling to larger volumes (such as the lymph nodes). When defining the present study, we also explored different methods of comparing isodoses to the WEPL re-calculations, including the Dice similarity coefficient. We found that the Dice coefficient was strongly biased by volume changes, unlike the target dose. Instead, we calculated the Hausdorff distances to all points in the iso-contours and the distal part in the iso-contours. We approached the data in multiple ways and found that the distance to the distal part had a stronger association with target dose degradation. We, therefore, decided to use a distance threshold and investigate the percentage of points within this threshold. This method makes it easier to judge if the range differences are within the uncertainty included in the planning, e.g. robustness settings and margins.

Our study showed that it was possible to detect target dose degradation based on range variations estimated from our WEPL calculations. WEPL changes might not directly capture the internal motion of the CTV. However, range variations based on WEPL-calculations can indirectly catch CTV-movement based errors, typically caused by anatomical changes, e.g. air

in the rectum, thereby altering the density in the beam path (figure 5). In clinical practice, rectal air may be overridden to tissue density during optimisation to make the plan more robust. The dose degradation in the p-CTV dose could be lesser in that case, although it would not account for the displacement of the target. Kim *et al* also found that differences in WEPL variations could reasonably capture the calculated dose/volume endpoints [13]. However, they explored it using the distal surface of the target volume. In contrast, our approach removed the need for the re-delineation of structures.

Automated segmentation of structures could enable the alternative of using direct dose calculations. However, this automation is still under development, with some TPSs offering experimental support. Most approaches to automated segmentation use a variant of machine learning (ML) [22, 23]. While ML-based methods are efficient, they can only be as good as the input data [24, 25]. ML-based segmentation is considered chiefly a black-box solution and will therefore require quality assurance and manual corrections [26].

The benefits of using WEPL calculations as an indicator for potential dose deterioration instead of a fully-fledged dose re-calculation are its simplicity and the speed of the calculation, in the order of milliseconds, and still highly parallelisable. These benefits make the range-guidance methods attractive for a busy clinical workflow. Although newer approaches to dose calculation improve on the required time [27, 28], fast dose re-calculation is not yet widely available. However, WEPL should not replace dose calculation but rather be used as a tool to indicate if dose re-calculation or re-planning might be needed. This tool must be sensitive, i.e. dose degradations are indeed flagged. Comparatively, the specificity is less important, although both high sensitivity and specificity would be preferred if possible. A WEPL-based method like the one we have introduced here also opens possibilities for more advanced range-guidance techniques. These techniques include robustness analysis [9, 10, 29], adaptive strategies and plan re-optimisation [30], or even adjusting patient positioning based on a dose re-calculation to account for anatomical changes [6, 7]. The clinical implementation of online daily adaptation in PT is essential to consider inter-fractional organ motion properly [3].

Incorporating range guidance into a clinical setting requires a volumetric image scan of the patient before treatment, e.g. a CBCT. However, CBCTs may contain inaccurate HUs, primarily due to scattered radiation. Multiple studies have explored different methods using either deformable image registration, making it possible to create a virtual CT or using a scatter-correction method with *a priori* information [31–33]. A scatter-corrected CBCT makes it possible to explore range guidance before treatment and assess the impact of inter-fractional organ motion on dose distribution. In future work, we will explore scatter-corrected CBCT for evaluating daily dose delivery with range guidance. The methods presented here should apply to any tumour site. However, each site with its respective beam configurations may see different correlation strengths between dose and range differences, so each site should be evaluated accordingly. A nationwide randomised clinical photon versus proton trial for locally advanced prostate cancer is currently being planned in Denmark, designed to investigate if PT reduces normal tissue toxicity compared to conventional photon-based RT. The WEPL-based evaluation method studied here will be further investigated within the frame of this trial.

Conclusion

This study investigated range guidance using WEPL calculations to detect target dose degradations in PT originating from internal organ motion. The iso-WEPLs were comparable to a dose re-calculation based on isodoses in the rCTs. In addition, target dose degradations were detected based on range guidance without the need for any re-delineation. Range guidance based on WEPL calculations could be an alternative to a fully-fledged dose re-calculation to detect severe anatomical variations and has the potential for further investigation as an indicator for adaptive PT strategies.

Data availability statement

The data generated and/or analysed during the current study are not publicly available for legal/ethical reasons but are available from the corresponding author on reasonable request.

ORCID iDs

Andreas G Andersen https://orcid.org/0000-0003-2868-0661
Jørgen B B Petersen https://orcid.org/ 0000-0001-9225-876X
Heidi S Rønde https://orcid.org/0000-0002-2736-8433
Sara Pilskog https://orcid.org/ 0000-0002-3475-7939
Ludvig P Muren https://orcid.org/ 0000-0002-7418-5832

References

[1] Thörnqvist S *et al* 2013 Degradation of target coverage due to inter-fraction motion during intensity-modulated proton therapy of prostate and elective targets *Acta Oncol.* **52** 521–7
[2] Szeto Y Z *et al* 2016 Effects of anatomical changes on pencil beam scanning proton plans in locally advanced NSCLC patients *Radiother. Oncol.* **120** 286–92
[3] Albertini F *et al* 2020 Online daily adaptive proton therapy *Br. J. Radiol.* **93** 20190594
[4] Nenoff L *et al* 2019 Daily adaptive proton therapy–the key to innovative planning approaches for paranasal cancer treatments *Acta Oncol.* **58** 1423–8

[5] Jagt T et al 2018 An automated planning strategy for near real-time adaptive proton therapy in prostate cancer Phys. Med. Biol. 63 135017
[6] Busch K et al 2019 On-line dose-guidance to account for inter-fractional motion during proton therapy Phys Imaging Radiat Oncol. 9 7–13
[7] Kurz C et al 2019 Dose-guided patient positioning in proton radiotherapy using multicriteria-optimization Z. Med. Phys. 29 216–28
[8] Gorgisyan J et al 2017 Impact of beam angle choice on pencil beam scanning breath-hold proton therapy for lung lesions Acta Oncol. 56 853–9
[9] Casares-Magaz O et al 2014 A method for selection of beam angles robust to intra-fractional motion in proton therapy of lung cancer Acta Oncol. 53 1058–63
[10] Andersen A G et al 2017 Beam angle evaluation to improve inter- fraction motion robustness in pelvic lymph node irradiation with proton therapy Acta Oncol. 56 846–52
[11] Kim J et al 2020 Beam angle optimization using angular dependency of range variation assessed via water equivalent path length (WEPL) calculation for head and neck proton therapy Phys Med. 69 19–27
[12] Santiago A et al 2015 Changes in the radiological depth correlate with dosimetric deterioration in particle therapy for stage i NSCLC patients under high frequency jet ventilation Acta Oncol. 54 1631–7
[13] Kim J et al 2017 Water equivalent path length calculations using scatter-corrected head and neck CBCT images to evaluate patients for adaptive proton therapy Phys. Med. Biol. 62 59–72
[14] Andersen A G et al 2020 Evaluation of an a priori scatter correction algorithm for cone-beam computed tomography based range and dose calculations in proton therapy Phys Imaging Radiat Oncol. 16 89–94
[15] Park Y-K and Andersen A G 2022 Gitlab source code repository (https://gitlab.com/agravgaard/cbctrecon)
[16] McCormick M et al 2014 ITK: Enabling reproducible research and open science Front Neuroinform. 8 13
[17] Hysing L B et al 2011 A coverage probability based method to estimate patient-specific small bowel planning volumes for use in radiotherapy Radiother. Oncol. 100 407–11
[18] Thörnqvist S et al 2011 Plan robustness of simultaneous integrated boost radiotherapy of prostate and lymph nodes for different image-guidance and delivery techniques Acta Oncol. 50 926–34
[19] Busch K et al 2021 Anatomical robust proton therapy using multiple planning computed tomography scans for locally advanced prostate cancer Acta Oncol. 60 598–604
[20] Andersen A G et al 2015 A method for evaluation of proton plan robustness towards inter-fractional motion applied to pelvic lymph node irradiation Acta Oncol. 54 1643–50
[21] Quan E M et al 2013 Preliminary evaluation of multifield and single-field optimization for the treatment planning of spot-scanning proton therapy of head and neck cancer Med. Phys. 40 081709
[22] Ren J et al 2021 Comparing different ct, pet and mri multi-modality image combinations for deep learning-based head and neck tumor segmentation Acta Oncol. 60 1399–406
[23] Guo Z, Guo N and Gong K 2019 Gross tumor volume segmentation for head and neck cancer radiotherapy using deep dense multi-modality network Phys. Med. Biol. 64 205015
[24] Vinod S K et al 2016 A review of interventions to reduce inter-observer variability in volume delineation in radiation oncology J Med Imaging Radiat Oncol 60 393–406
[25] Bondue C, Racadot S and Coutte A 2019 Volumetric and dosimetric comparison of two delineation guidelines for the radiation treatment of laryngeal squamous cell carcinoma Clin Transl Radiat Oncol 19 1–11
[26] Rigaud B et al 2021 Automatic segmentation using deep learning to enable online dose optimization during adaptive radiation therapy of cervical cancer Int. J. Radiat. Oncol. Biol. Phys. 109 1096–110
[27] Jia X et al 2012 GPU-based fast Monte Carlo dose calculation for proton therapy Phys. Med. Biol. 57 7783–97
[28] Qin N et al 2016 Recent developments and comprehensive evaluations of a GPU-based Monte Carlo package for proton therapy Phys. Med. Biol. 61 7347–62
[29] van der Voort S et al 2016 Robustness recipes for minimax robust optimization in intensity modulated proton therapy for oropharyngeal cancer patients Int J Radiation Oncol Biol Phys. 95 163–70
[30] Botas P et al 2018 Online adaption approaches for intensity modulated proton therapy for head and neck patients based on cone beam CTs and Monte Carlo simulations Phys. Med. Biol. 64 015004
[31] Landry G et al 2015 Investigating CT to CBCT image registration for head and neck proton therapy as a tool for daily dose recalculation Med. Phys. 42 1354–66
[32] Park Y-K et al 2015 Proton dose calculation on scatter-corrected CBCT image: Feasibility study for adaptive proton therapy Med. Phys. 42 4449–59
[33] Kurz C et al 2016 Investigating deformable image registration and scatter correction for CBCT-based dose calculation in adaptive IMPT Med. Phys. 43 5635–46